A teleseismic finite-fault rupture model for the August 17, 1999, İzmit earthquake (*Mw* = 7.6): implications for the seismic nucleation phase

Murat Utkucu and Hatice Durmuş[*]

Sakarya University, Esentepe Campus, Department of Geophysics, Sakarya, Turkey

ABSTRACT

A linear finite-fault inversion procedure is applied to teleseismically recorded broadband P *and* SH *velocity waveforms of the August 17, 1999, İzmit earthquake, to derive spatial and temporal distributions of the co-seismic slip over the representative three-segment model fault. The model fault is longer than the mapped surface rupture, and it extends offshore for 25 km in the west, to define the western end of the earthquake rupture. The teleseismically derived slip model suggests a bilateral rupture with a total seismic moment release of 2.6 ×10²⁰ Nm, and that the rupture was dominated by failure of two major asperities with peak slip amplitudes reaching 7 m. The hypocentral area was represented by the relatively low displacement that separated the large asperities. In the west, the rupture reached the eastern entrance of the Çınarcık basin beneath the Sea of Marmara, with an average slip of ca. 2 m. This indicates that the rupture propagated offshore for ca. 20 km after crossing Hersek Peninsula. The analysis also reveals that the total rupture process time was 32 s, while the main seismic moment release, which corresponded to the rupture of the two large asperities, occurred between 4 s and 16 s after rupture initiation. The strong wave energy arrivals from the failure of the large asperities were preceded by weak wave arrivals in the initial section of the teleseismic waveforms used in this study. Along with some observations from previous studies, this emergent onset of the wave arrivals prompts us to discuss the possibility of a seismic nucleation process for this earthquake.*

1. Introduction

The North Anatolian Fault Zone (NAFZ) is a 1,500-km-long dextral transform fault that extends from Karlıova Triple Junction in the east to the northern Aegean Sea in the west [Barka and Kadinsky-Cade 1988, Şengör et al. 2005] (Figure 1). It accommodates western extrusion of the Anatolian plate, which is caused by the regional plate kinematics, along with the sinistral East Anatolian Fault Zone [Barka and Kadinsky-Cade 1988, McClusky et al. 2000, Reilinger et al. 2006]. Karlıova Triple Junction marks the junction of both transforms. The global positioning system (GPS)-derived crust velocity field has indicated that virtually all of the relative motion of the Eurasian–Anatolian plate was along the NAFZ, with a slip-rate of about 24 mm/yr. Virtually no internal deformation was observed within central Anatolia [McClusky et al. 2000, Reillinger et al. 2006].

The extent of the NAFZ from Karlıova Triple Junction to NW Turkey can be approximated by a single fault trace. However, in NW Turkey, it bifurcates into two fault strands, the northern and southern strands, and there is an asymmetric partitioning of the slip rate in this region (Figure 2) [Barka and Kadinsky-Cade 1988, Armijo et al. 2002, Meade et al. 2002, Flerit et al. 2003, Nyst and Thatcher 2004]. It has been shown that the northern strand showed a much larger slip rate, at 20 mm/yr, with the rest of the slip rate along the southern strand. Both of these strands have resulted in remarkable seismic activity, with tens of large destructive earthquakes through history [Ambraseys and Finkel 1991, Ambraseys 2002], which are exemplified by the destructive August 17, 1999, İzmit (*Mw* 7.6) and November 12, 1999, Düzce (*Mw* 7.1) earthquakes (Figure 2).

The NAFZ produced a sequence of six large earthquakes, which migrated westwards in both time and space [Toksöz et al. 1979, Barka 1996, Şengör et al. 2005] (Figure 1). Each of the earthquake ruptures triggered the next rupture through Coulomb static-stress loading [Stein et al. 1997]. The notorious August 17, 1999, İzmit (*Mw* 7.6) earthquake was apparently the last case in the westward migration of these earthquake ruptures, and it had unprecedented social and economical impact on modern Turkey [Barka et al. 2002, Şengör et al. 2005] (Table 1, Figure 2). The fault segments that produced the 1999 İzmit earthquake were mostly stressed by the earlier earthquakes of the westwards migrating sequence, with the implication of increasing probability of an earthquake rupture [Stein et al. 1997, Lorenzo-Martin et al. 2006].

The 1999 İzmit earthquake produced well-developed, multi-segmented, 110-km-long, directly observable and almost pure dextral surface ruptures that extended mostly onshore between Gölyaka and Gölcük, and mostly offshore westwards from Gölcük (Figures 2, 3) [Barka et al. 2002,
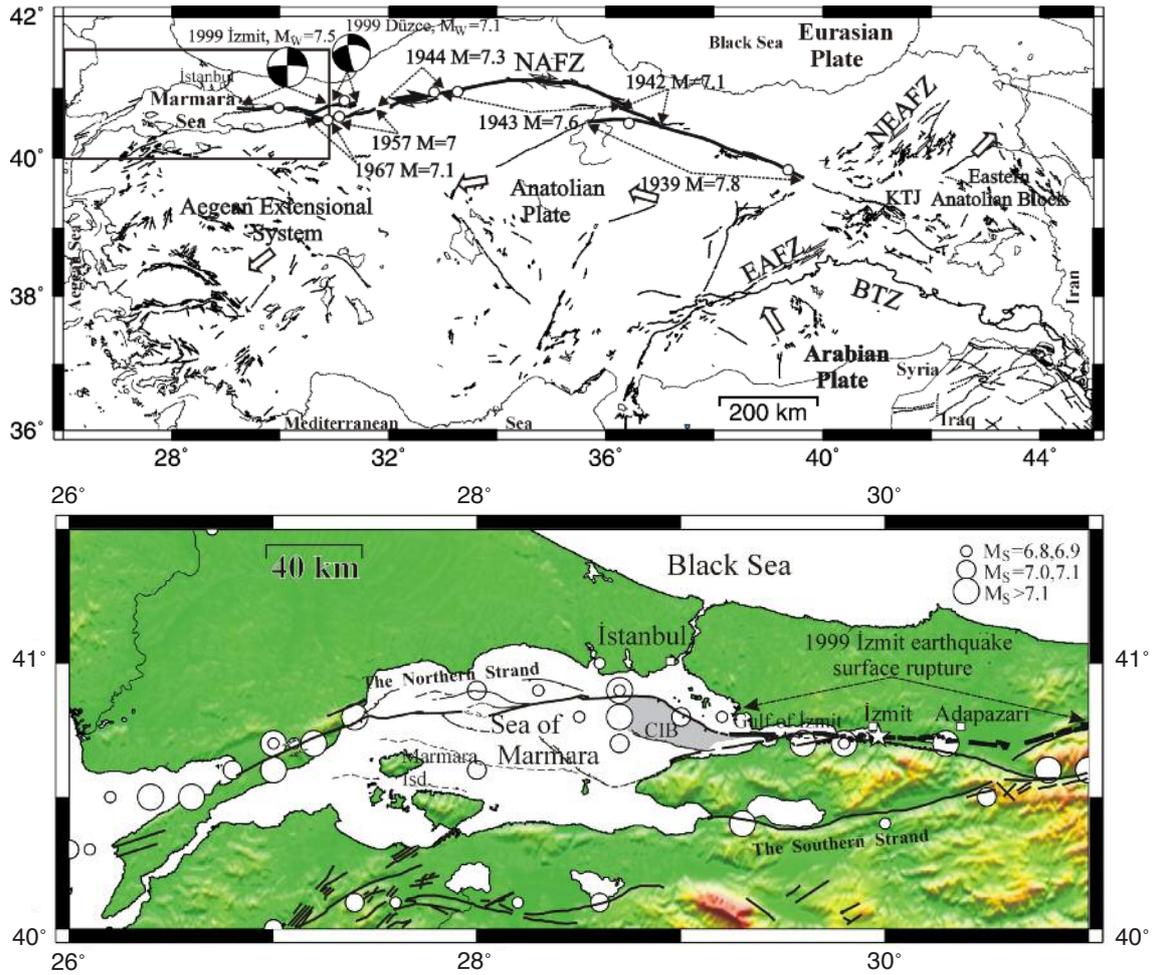
Figure 1 (top). Map showing the major tectonic settings of Turkey and the westward space-time migration of the large earthquake ruptures along the North Anatolian Fault Zone (NAFZ) between 1939 and 1999, as well as the focal mechanisms (black and white beach balls) of the August 17, 1999, İzmit and November 12, 1999, Düzce earthquakes (compiled from Şaroğlu et al. [1992], Barka et al. [2002], Tibi et al. [2001]). Open circles, earthquake epicentres; large arrows, plate motions relative to the stable Eurasian Plate; large rectangle, the map area shown in Figure 2. EAFZ, East Anatolian Fault Zone; NEAFZ, North-East Anatolian Fault Zone; KTJ, Karlıova Triple Junction; BTZ, Bitlis Thrust Zone.

Figure 2 (bottom). Map showing the extent of the North Anatolian Fault Zone (NAFZ) in NW Turkey, along with the epicenters of $M_S \geq 6.8$ earthquakes (white filled circles) after 400 AD [Şaroğlu et al. 1992, Ambraseys 2002]. The extent of the NAFZ beneath the Sea of Marmara is after Armijo et al. [2002]. The extent of the surficial ruptures of the August 17, 1999, İzmit earthquake are also shown (thick black lines). Gray filled area, Çınarcık Basin (CIB). See Figure 3 for a larger scale map and for detailed information of the surficial ruptures.

Parameter	KOERI[1]	ÖZ[2]	TI[3,a]	Harvard CMT	USGS	ISC	RE[4,b]	Gülen et al. [2002][a]	Delouis et al. [2002][c]	Li et al. [2002][a]
Lat. (°)	40.770	40.729		41.010	40.748	40.756				
Long. (°)	29.960	29.967		29.970	29.864	29.955				
Depth (km)	10	13		17	13	17				
$M_o \times 10^{20}$ Nm			1.47	2.88	1.4		1.7	2.42	2.4	1.3
Strike (°)			270	182	185					90
Dip (°)			83	74	90					90
Rake (°)			181	3	9					−180

[1] Kandilli Observatory and Earthquake Research Institute.

[2] Özalaybey et al. [2002].

[3] Tibi et al. [2001].

[4] Reilinger et al. [2000].

[a] From the inversion of the teleseismic P and SH waveforms.

[b] From the modeling of the GPS data.

[c] From the inversion of the strong-motion, teleseismic, InSAR and GPS data.

Table 1. The hypocentral and source parameters of the August 17, 1999, İzmit earthquake estimated by different seismological organizations and previous studies.
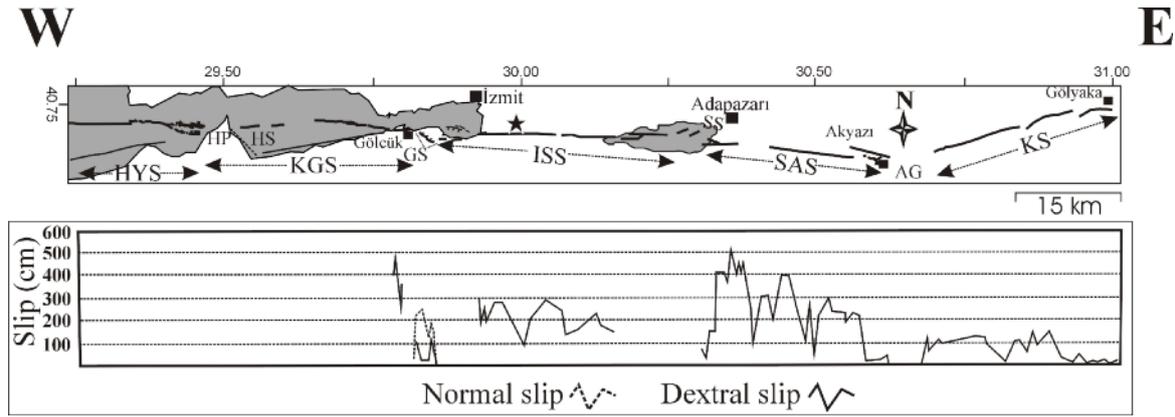
Figure 3. The surface ruptures of the 1999 İzmit earthquake (thick black lines), as mapped from the field and submarine geology studies (above) and surface displacements measured along the surface ruptures (compiled from Barka et al. [2002], Lettis et al. [2002], Armijo et al. [2002], Cormier et al. [2006]). The earthquake was due to rupture of five fault segments, namely from east to west: the Karadere (KS), Sapanca-Akyazı (SAS), İzmit-Sapanca (ISS), Karamürsel-Gölcük (KGS) and Hersek-Yalova (HYS) segments along the North Anatolian Fault Zone. Black star, epicentre of the 1999 İzmit earthquake. AG, Akyazı Gap; SS, Sapanca stepover; GS, Gölcük stepover; HS, Hersek stepover; HP, Hersek Peninsula.

Lettis et al. 2002, Gülen et al. 2002, Aydın and Kalafat 2002, Armijo et al. 2005]. Field observations have shown that the earthquake rupture comprised five right-stepping fault segments (from east to west, across the Karadere [KS], Sapanca-Akyazı [SAS], İzmit-Sapanca [ISS], Karamürsel-Gölcük [KGS] and Hersek-Yalova [HYS] segments) that were separated by the geometrical discontinuities of the Akyazı Gap and Sapanca, Gölcük and Hersek releasing stepovers (Figure 3). The vertical displacement was locally dominant along the 3-km-long Gölcük fault within the Gölcük stepover formed between HYS and KGS. Maximum dextral surface displacements (about 5 m) were measured along SAS and KGS (Figure 3). A peak vertical displacement of 2.3 m was reported along the Gölcük fault. With the exception of the easternmost KS, which strikes N65°E, all of the ruptured segment has a roughly EW strike. Source mechanism studies for this earthquake indicate almost pure dextral faulting along a roughly EW trending, northerly dipping, and nearly vertical nodal plane (Table 1, Figure 1).

The rupture properties of this 1999 İzmit earthquake have been studied extensively through modeling of the seismic waveforms and geodetic data (Table 1, Figures 1, 4). Sekiguchi and Iwata [2002] and Bouchon et al. [2002] inverted the strong-motion waveforms, while Tibi et al. [2001], Gülen et al. [2002] and Li et al. [2002] inverted the teleseismic displacement waveforms, to reveal the source rupture process. Reilinger et al. [2000] modeled GPS data to reveal the coseismic and post-seismic slip that was associated with this earthquake. Çakır et al. [2003] mapped the coseismic and post-seismic slip over the rupture plane using both InSAR and GPS data. Individual and joint inversions of the strong-motion, teleseismic, InSAR and GPS data were carried out by Delouis et al. [2002]. Vallee and Bouchon [2004] constructed a rupture model that was based on the teleseismic body and surface waves. These studies have been mostly in agreement and have revealed that: 1) the rupture was bilateral, with mostly eastwards propagation, and

the main rupture of the 1999 İzmit earthquake extended from 10 km west of Gölcük to 10 km west of Akyazı, over the SAS, ISS and KGS fault sections; 2) two prominent slip areas, or asperities, have peak slip values exceeding 5 m and straddle the hypocenter; 3) the main rupture was strongly perturbed by the Hersek releasing stepover in the west, such that the slip amplitude fell off and terminated after propagating 10 km to 20 km westwards (Figures 3, 4).

The aim of the present study is to carry out finite-fault modeling of the teleseismic *P* and *SH* velocity waveforms of the 1999 İzmit earthquake through a least-squares inversion scheme, for the spatial and temporal distribution of the coseismic slip. Although teleseismic displacements have been used in previous studies, no study has been carried out so far using teleseismic velocity recordings. The teleseismic velocity waveforms are more sensitive to the time evolution of an earthquake rupture than teleseismic displacements, and more sensitive to the overall rupture pattern than strong-motion records, and they contain information about the coseismic slip history, to which geodetic data is blind. The present study is also aimed at a comparison of the rupture model based on the teleseismic velocities with previously proposed models, and at further discussion of the coseismic rupture of the earthquake a decade after its occurrence. The 1999 İzmit earthquake promoted stress levels beyond both ends of its rupture [Parsons et al. 2000, Hubert-Ferrari et al. 2000, Utkucu et al. 2003, Parsons 2004, Pondard et al. 2007]. The stress load triggered the 1999 Düzce (*M*w = 7.1) earthquake 3 months later, and advanced the occurrence of possible event(s) along the fault segments lying beneath the eastern Sea of Marmara, which is known to be a seismic gap. There is no doubt that a better understanding of the finite fault properties of the 1999 earthquake, such as the location of its western termination and the slip contributions of each ruptured segment, will be important for accurately estimating the seismic hazard in the eastern Sea of Marmara.
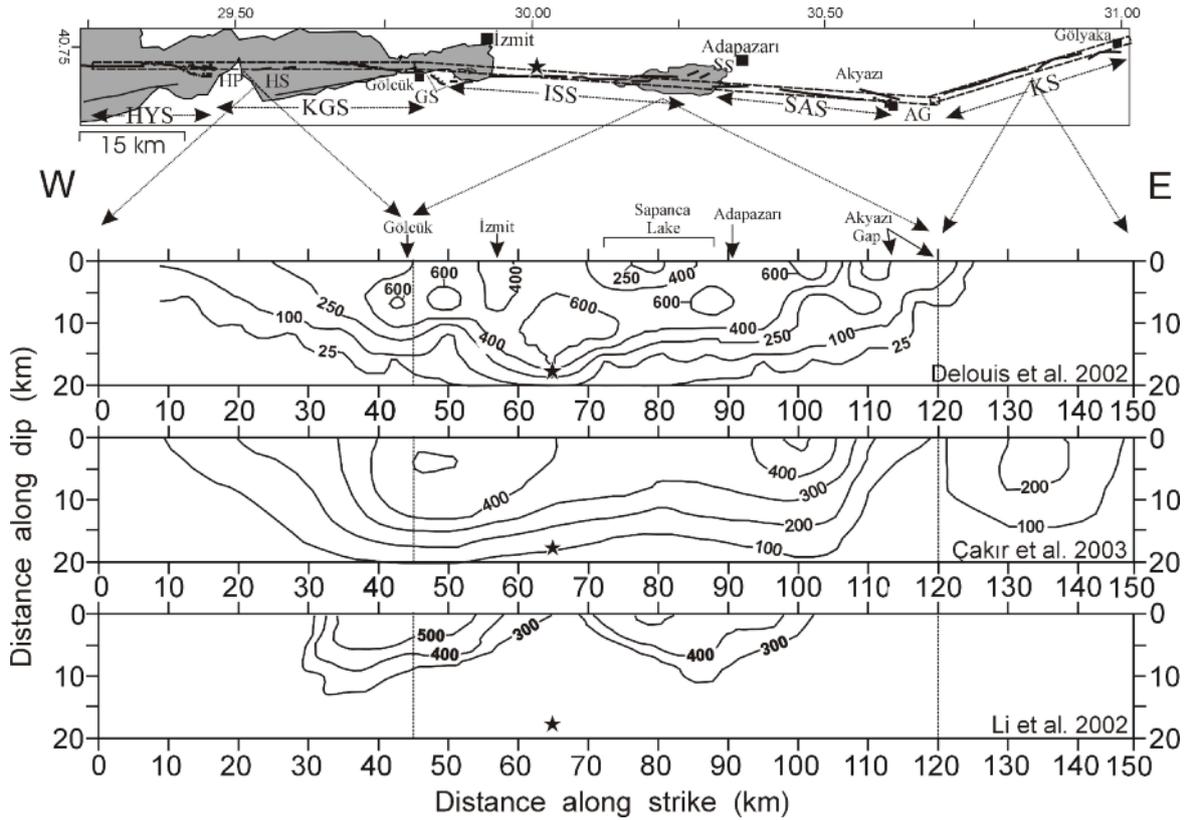
Figure 4. Slip models of the 1999 İzmit earthquake arising from earlier studies. The slip model of Deluois at al. [2002] was recovered from joint inversion of the seismic waveforms (near-field + teleseismic) and geodetic data (GPS + InSAR). Çakır et al. [2003] inverted the geodetic data (GPS + InSAR), while Li et al. [2002] modeled teleseismic displacement waveforms. The map of the surface rupture extent for correlating the slip distribution in the depth with the surface rupture trace is also shown. See caption of Figure 3 for abbreviations. Solid star, hypocenter used in the present study.

2. Finite-fault modeling

2.1. Data processing

We used teleseismic broadband *P* and *SH* body waveforms for the 1999 İzmit earthquake that were retrieved from the Incorporated Research Institutes for Seismology (IRIS) Data Management Center (http://www.iris.edu). The observed data comprise 25 *P* and 15 *SH* waveforms, with epicentral distances between 32° and 90° for the *P* waveforms, and 39° and 82° for the *SH* waveforms. The selections of these epicentral ranges were made to avoid upper-mantle distortions and core-mantle boundary diffractions in the waveforms. The stations included in the present study provide good azimuthal coverage around the source.

Taking into account the observed rupture length, the rupture extent with regard to the epicenter location, and the finite-fault model parameterization used in the present study (Figure 5), a record length of 50 s was used for both the *P* and *SH* waveforms. This time window is sufficient for mapping all of the coseismic slip contribution from a rupture plane extending from the eastern termination of the rupture in the south of Gölyaka to 20 km west of Hersek peninsula in the west, and covering 20 km of the uppermost crust. By comparing teleseismic displacement *P* waveforms of the mainshock with the largest aftershock of September 13, 1999, which was located in the near vicinity of the

mainshock hypocenter, Li et al. [2002] showed that despite the coupling with the scattered wave energy in the later part of the first 45 s of the *P* wavetrain, this time window includes mainly source radiation. We inverted the velocity waveforms rather than the displacement waveforms used in previous teleseismic source studies [e.g. Li et al. 2002, Gülen et al. 2002, Delouis et al. 2002]. The original data were corrected for the instrument responses, to obtain true ground velocities, and bandpass filtered with corner frequencies at 0.01 Hz to 0.5 Hz. A sampling interval of 0.20 s was used in the finite-fault inversions.

2.2. Method and model parameterization

A finite-fault waveform inversion was used in the present study, which was originally developed by Hartzell and Heaton [1983] and has been widely used for studying earthquake rupture properties [e.g. Hartzel et al. 1991, Mendoza 1993, Wald and Heaton 1994, Mendoza 1995, Langer and Harzell 1996]. The method will be briefly discussed here, and readers are referred to Hartzell and Heaton [1983] and Wald and Heaton [1994] for detailed explanation.

First, the application requires the source of the earthquake to be represented by a two-dimensional model fault plane. The length, width and orientation of the model fault plane are defined through consideration of the available geological or seismological information of the relevant

Figure 5. Finite-fault model parameterization used to obtain the slip distribution of the 1999 İzmit earthquake, along with the mapped surface ruptures. The three-segment model fault has a total length of 150 km, a width of 20 km, a dip 85°N and is discretized as 120 square subfaults, with 5 km along each side. Solid stars, hypocenter; broken line rectangles in the map, surface projections of the model fault segments. The names and strikes of the fault segments adopted in the text and used in the modeling are also shown, respectively. See caption of Figure 3 for abbreviations used in the map.

earthquake, such as the magnitude, focal mechanism, aftershock distribution, and mapped surface ruptures. As described above, the mapped surface ruptures of the 1999 İzmit earthquake include five fault segments that showed different strikes and extended for 110 km onshore, with a possible offshore extension also a matter of debate. The distributions of the well-located aftershocks [Özalaybey et al. 2002], the modeling of the geodetic data [Reilinger et al. 2000, Delouis et al. 2002, Çakır et al. 2003], and the clear morphologic evidence found in the sea bottom [Armijo et al. 2005] all require a fault rupture that is above the depth of 20 km in the crust and that extends well offshore of the Hersek Peninsula, to the eastern entrance of the Çınarcık Basin (Figure 2). Therefore, we used a three-segment model fault to approximate the varying strike of the ruptured segments that extend from Gölyaka in the east to the eastern entrance of the Çınarcık Basin in the west, which measures

150 km in length (Figure 5). From east to west, the three model fault segments (named as the eastern, central and western segments) strike 250°, 274° and 270°, respectively, with the same dip angle of 85°N. By extending the model fault west of the Hersek Peninsula, we also explore the location of the western termination of the rupture in the modeling. The width of the model fault is taken as 20 km. The model fault is then divided into 120 equal-sized 5 km × 5 km square subfaults (with 30 along the strike, and 4 along the dip) for spatial distribution of the coseismic slip. Thirty-six point sources are evenly distributed over each subfault (with a point-source spacing of 1 km along the strike and down-dip direction), for simulation of the radial propagation of the rupture from the hypocenter. The model fault plane is placed in the earthquake source structure so that its top edge roughly aligns with the mapped surface rupture and its western tip is 65 km from the epicenter coordinates

determined by Özalaybey et al. [2002] (Table 1, Figure 5). The vertical projection of the epicenter intersects with the fault plane at a hypocentral depth of 17 km, and the fault plane extends from the free surface to a depth of ca. 19.9 km.

Generalized ray theory [Langston and Helmberger 1975] is used for the calculations of the point-source responses, with a crustal velocity structure based on the study of Horasan et al. [2002] (Table 2). The point sources are appropriately lagged in time to represent radial propagation of the rupture from the hypocenter and to allow for travel-time differences between each source–station pair. The point source responses are then summed to construct subfault synthetic seismograms (i.e. Green's functions) for each station included in the inversion. Attenuation is incorporated by the convolution of subfault synthetics with a constant attenuation operator, t*, of 0.7 s for the *P* waves and 4 s for the *SH* waves. The subfault synthetics are bandpass filtered for the same frequency range, and sampled for the same time interval as the observations.

A rupture velocity and a source time function are also described for the generation of the synthetics. Using a fixed rupture velocity and a source time function can yield a slip model that is insufficient in terms of the finite fault properties of large and complex earthquakes. Therefore, flexibility in the rupture velocity and source time function was allowed for by using a multiple time window approach to allow for locally variable rupture velocities and complicated source time functions over the model fault plane [Hartzell and Heaton 1983, Wald and Heaton 1994, Mendoza 1995]. We incorporated five consecutive time windows in the finite-fault modeling and the source time function of each time-window is represented by an isosceles triangle with a 1-s rise and fall. Each time window is lagged 2 s from the previous one, so that they do not overlap, allowing the longer slip duration of 10 s for each point over the fault. From the inversion of the strong-motion data, Bouchon et al. [2002] showed that the slip rise time over the fault plane is ≤5 s, and is mostly in the range of 3 s to 5 s. Therefore, allowed flexibility in the slip duration is considered to be sufficient for this earthquake.

Although the multiple time window approach allows a variable rupture velocity, we need to define a maximum rupture velocity to be allowed in the modeling. A supershear rupture velocity of about 4.8 km/s is proposed for the main rupture area of the 1999 İzmit earthquake between İzmit and Adapazarı (Figure 3), regarding the short *S-P* time observed at the SKR strong-motion station at Adapazarı [Ellswoth and Çelebi 1999, Bouchon et al. 2002]. However, a supershear rupture velocity along a section of the rupture plane has been a matter of debate. The dynamic triggering of an asperity, which is located between the hypocenter and Adapazarı, by *P* waves leaving the hypocenter has also been proposed to explain the short *S-P* time observed at SKR [Anderson et al. 2000]. Using strong-motion data, Sekiguchi and Iwata [2002] were not able to distinguish among three possibilities: a supershear rupture, the *P*-wave triggering of an asperity, or a combination of these. Teleseismic waveform inversion studies, however, have shown that the teleseismic data do not require a supershear rupture velocity [Delouis et al. 2002, Li et al. 2002]. Delouis et al. [2002] successfully modeled the teleseismic and strong-motion data with a maximum rupture velocity of 3.5 km/s, while Vallee and Bouchon [2004] reported that a mean rupture velocity of 2.3 km/s largely explained the teleseismic data and Love wave relative source time functions derived by empirical Green's function analysis using the largest aftershock. Regarding this debate, we tried several maximum rupture velocities for individual segments of the model fault to find the maximum rupture velocity values for the each segment that best explain the teleseismic velocity data used in the present study.

The subfault synthetic records and the observed records define an over-determined system of linear equations of the form $\mathbf{A}\mathbf{x} = \mathbf{b}$, where $\mathbf{A}$ is the matrix of the synthetics, $\mathbf{b}$ is the data vector, and $\mathbf{x}$ is the solution vector, which comprises the slip weights of each subfault such that the synthetics fit the observed data. The solution vector, $\mathbf{x}$, is solved by using a Householder least-squares inversion method [Lawson and Hanson 1974] that constrains each value of the solution vector to be ≥0. Smoothing and moment minimization constraints are also imposed on the inversion, to find a slip model with a smooth distribution of slip and with minimum seismic moment [Hartzell and Heaton 1983, Wald and Heaton 1994].

3. Inversion results

As indicated above, several inversion trials have been conducted, to reveal the maximum rupture velocity of each segment that best explains the data. In the initial trial, maximum rupture velocities of 3.3 km/s, 3.5 km/s and 3.3 km/s were assigned to the eastern, central and western segments, respectively. In the following inversion trials, slower and higher rupture velocities than the initially assigned values for the central segment were used, while only slower rupture velocities than the initially assigned values were tried for the other segments. The value of $||\mathbf{b} - \mathbf{A}\mathbf{x}||$, the Euclidean

VP (km/s)	VS (km/s)	Density (kg/m3)	Thickness (km)
3.50	2.20	2000	4.0
5.80	3.40	2700	13.0
6.20	3.60	2800	15.0
8.00	4.60	3340	

Table 2. The crustal velocity structure used in the present study (modified from Horasan et al. [2002]).

Model	Rake (°)			V_r			M_0 $(\times 10^{20}\,\text{Nm})$	$\|b-ax\|$	Variance
	S_1	S_2	S_3	S_1	S_2	S_3			
M1	−180	−180	−180	3.3	3.5	3.3	2.64	27.191	0.07647398
M2	−180	−180	−180	3.3	3.7	3.3	2.69	27.237	0.07669328
M3	−180	−180	−180	3.3	3.9	3.3	2.72	27.223	0.07659071
M4	−180	−180	−180	3.3	3.3	3.3	2.61	27.250	0.07671893
M5	−180	−180	−180	3.3	3.1	3.3	2.56	27.343	0.07723550
M6	−180	−180	−180	3.1	3.1	3.1	2.73	27.340	0.07725047
M7	−180	−180	−180	2.9	2.9	2.9	2.46	27.372	0.07744742
M8	−180	−180	−180	3.3	4.1	3.3	2.75	27.410	0.07775906
M9	−175	−175	−175	3.3	3.5	3.3	1.20	33.661	0.11497340
M10	−180	−180	−180	3.3	5.0	3.3	2.83	27.473	0.07810884

Table 3. Finite-fault inversion trials carried out in the modeling of the August 17, 1999, İzmit earthquake. Note that the model M1 trial gives the minimum misfit error and residual variance.

norm of the misfit between the observed data and synthetics, and the variance values for these inversion runs, are shown in Table 3. The variances are estimated by dividing the square of the Euclidean norm by the number of degrees of freedom, which is defined as (n-1), where n is the number of data points in the inversion minus the number of non-zero model parameters [Hartzell and Iida 1990].

As can be seen from Table 3, the maximum rupture velocities defined for the initial trial (model M1) gave the minimum misfit error and residual variance. Then another inversion run with a rake angle of −175° was also tried (model M9). This trial resulted in a much degraded fit to the data than for model M1, with rake angle of −180°. Therefore

we consider model M1 as the most reliable representation of the earthquake fault rupture in the present study.

The slip model for the model M1 trial is shown in Figure 6a. A seismic moment of 2.6×10^{20} Nm ($M_W \approx 7.6$) is estimated for the slip model. The synthetic waveforms generated from the slip model are compared with the observed velocity waveforms in Figure 7, which indicates that a satisfactory fit between the synthetic and observed seismograms is achieved. As will be referred to in the following discussion of the results, in Figure 6b, we also show the slip distribution for model M10, in which a supershear rupture velocity of 5.0 km/s is adopted for the central segment of the model fault.
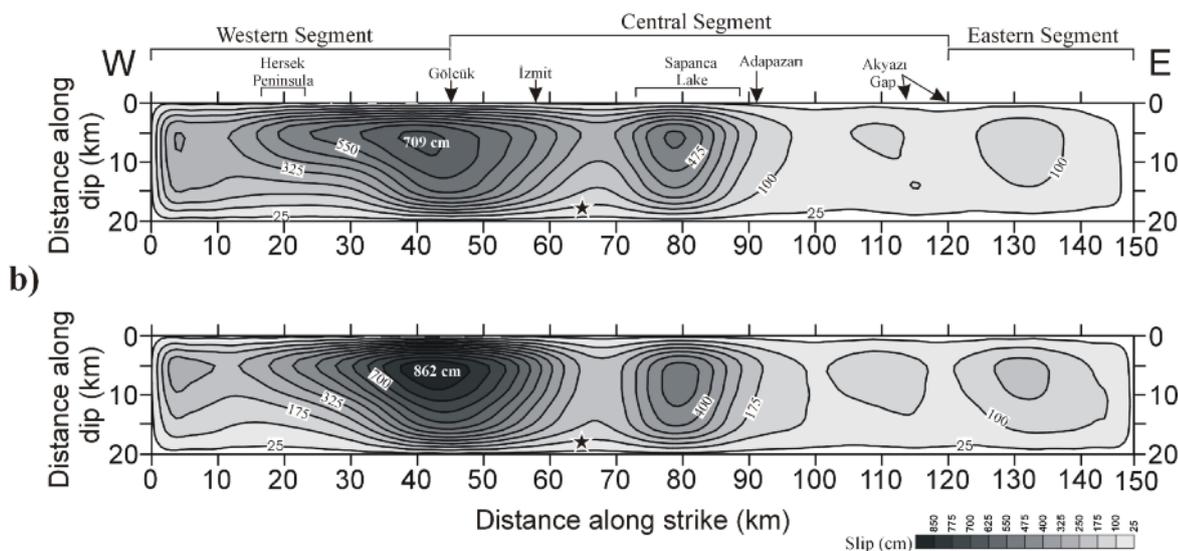

Figure 6. a) Contour map of the slip distribution that gives the best fit to the teleseismic velocity data and is assumed as the coseismic slip distribution model (model M1 in Table 3) of the 1999 İzmit earthquake in the present study. The central segment has a rupture velocity of 3.5 km/s while the other segments have a rupture velocity of 3.3 km/s. **b)** Contour map of the coseismic slip distribution of the 1999 İzmit earthquake arising from the present study, with the central segment of the model fault plane having a rupture velocity of 5 km/s, and the other segments having a rupture velocity of 3.3 km/s. This model corresponds to model M10 in Table 3. Note that slip larger than 25 cm is contoured at 75-cm intervals. Solid star, hypocenter. The projected locations of the towns of İzmit, Adapazarı, Gölcük, Akyazı, and the extent of Sapanca Lake and the Akyazı surface rupture gap along the strike are also shown.
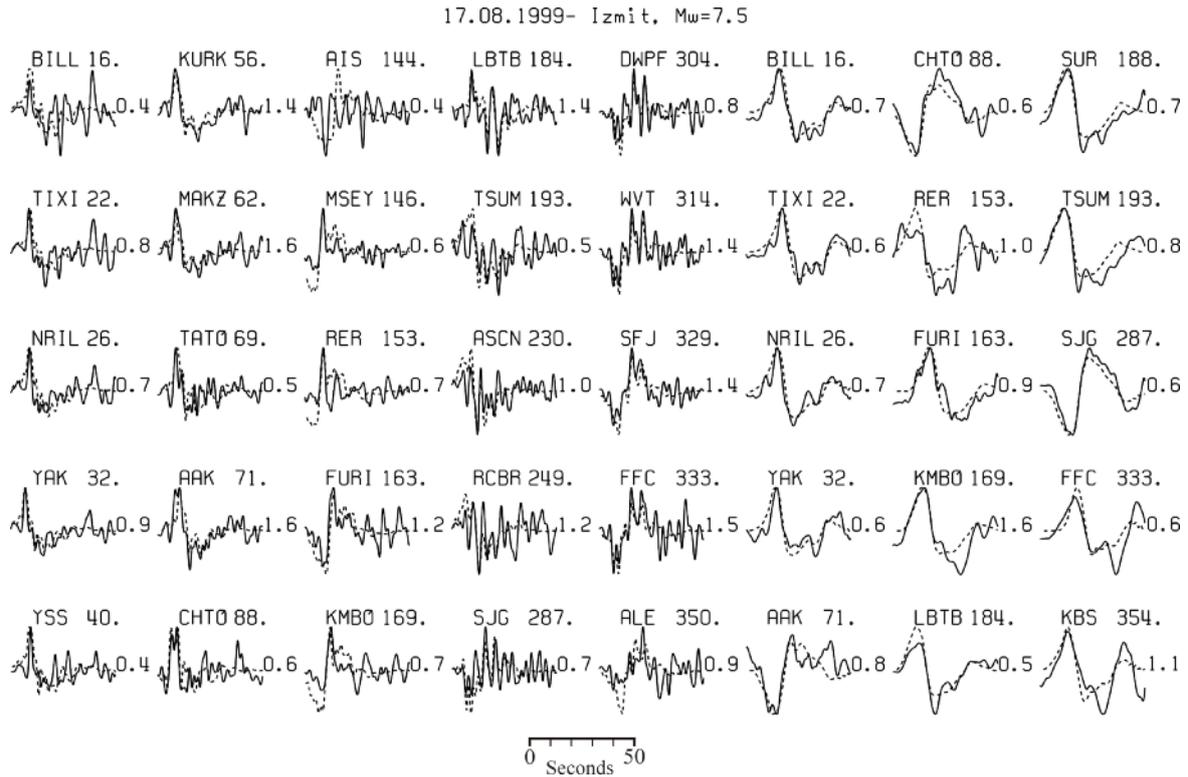
17.08.1999- İzmit, Mw=7.5

Figure 7. Comparisons of the observed waveforms (solid curves) and the synthetic waveforms (dashed curves) calculated for the slip model shown in Figure 6a. The station names and azimuths, clockwise from the North, are given on the top left and top right of each observed–synthetic waveform pair, respectively. The numbers to the right of each waveform pair indicate the synthetic-to-observed amplitude ratios.

4. Discussion

As can be seen from Figure 6a, the slip model for the 1999 İzmit earthquake suggests a very heterogeneous coseismic slip distribution and a bilateral rupture that mostly propagated eastwards. Most of the total seismic moment was released from the westward-propagating rupture. The coseismic slip model is dominated by the rupture of two large asperities, the eastern and western asperities, which cover a faulting area of 70 km in length between Adapazarı in the east, and Hersek Peninsula in the west. The hypocenter is located in a fault area between these large asperities, with relatively low slip (about 1 m), which constitutes another conspicuous property of the slip model.

The slip area of the eastern asperity is centered beneath the Sapanca Lake, at a depth of about 6 km, and up-dip east of the hypocenter, with a peak slip of ca. 5.5 m (Figure 6a). Its rupture lies mostly over ISS and across the western part of SAS. The western asperity is larger than the eastern asperity, both in its faulting area and its slip amplitude, which is about 7 m. The western asperity represents the rupture of the western part of ISS and KGS, and it has an elongated shape in the strike direction.

The slip associated with the eastwards rupture of the eastern asperity gradually diminishes in amplitude after crossing the Sapanca stepover. The slip amplitude over the western part of SAS that lies south of Adapazarı is roughly 2 m. The coseismic slip is barely above 1 m between Adapazarı and Akyazı, and almost vanishes over the fault area that remains between Akyazı and the western tip of KS, which matches the Akyazı Gap observed along the mapped surface ruptures. The rupture of KS represents the easternmost rupture during the earthquake, with a slip of about 1.5 m. The rupture jumps the Hersek stepover, and proceeds to HYS in the west, with a slip of about 2.5 m.

The slip model also indicates that the rupture propagated offshore west of Gölcük for about 40 km, to the eastern tip of the Çınarcık Basin (see Figure 2 for its location). This conclusion is also supported by direct morphological observations [Armijo et al. 2005, Gasperini et al. 2011], the teleseismic inversion [Gülen et al. 2002], and the geodetic analysis [Reilinger et al. 2000, Delouis et al. 2002, Çakır et al. 2003, Bos et al. 2004]. At the eastern entrance of the Çınarcık Basin along HYS, Armijo et al. [2005] found well-preserved fresh fault breaks, which they attributed to the 1999 İzmit earthquake rupture. Using high-resolution seismic reflection profiles, acoustic imagery, and direct underwater observation carried out with remotely operated vehicles, Gasperini et al. [2011] concluded that the surface rupture of the 1999 İzmit earthquake propagated along HYS and tapered out before reaching Çınarcık Basin. Uçarkuş et al. [2011] studied the microbathymetry data, and suggested that the 1999 İzmit earthquake extended about 10 km west of Hersek Peninsula, to reach a total rupture length of 145 km. The rupture of HYS corresponds to sub-event 4 that resulted from the teleseismic rupture process analysis of Gülen et al. [2002], with 1.3 m slip. By analyzing InSAR and
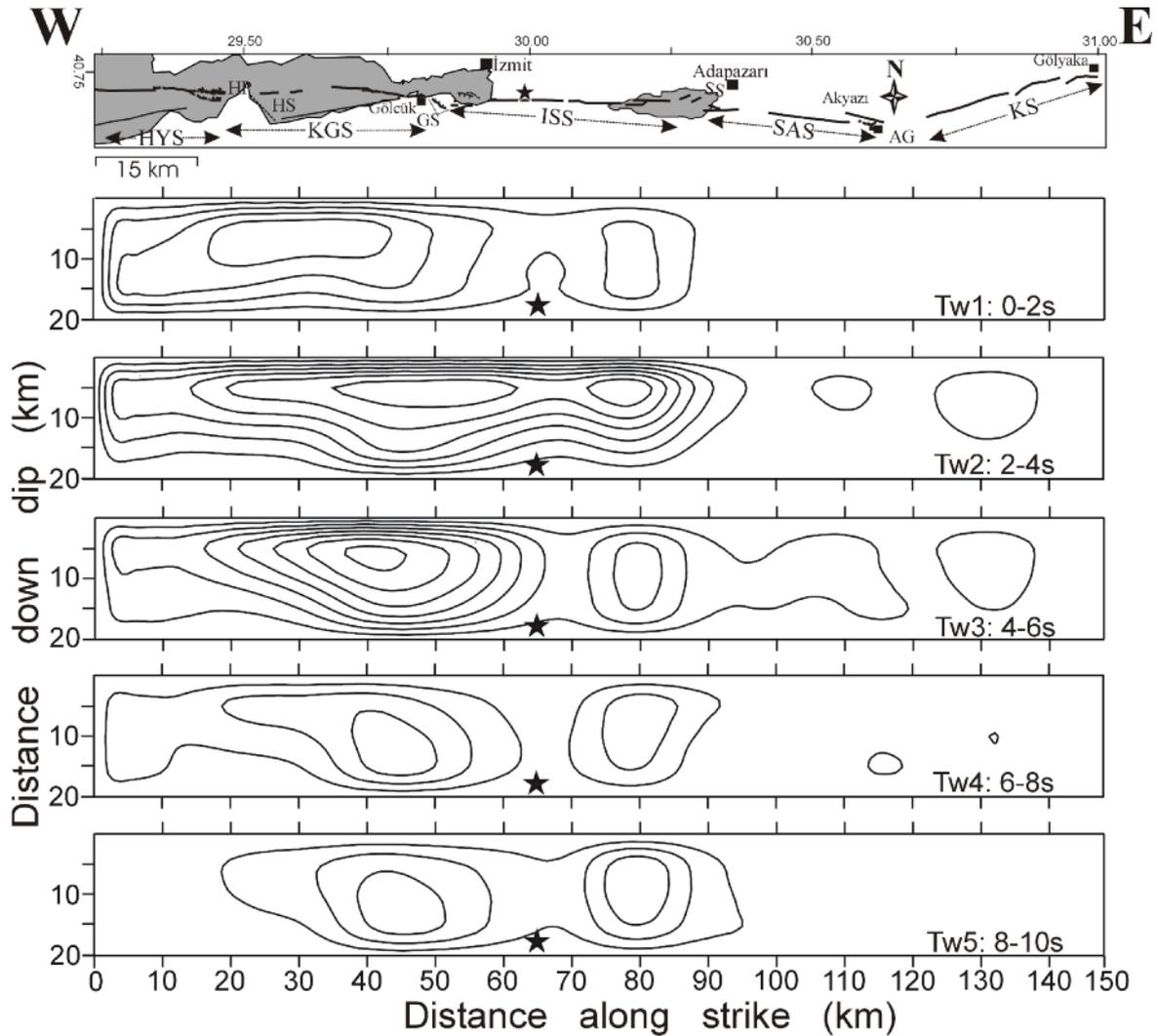
Figure 8. Individual slip contributions of each time window to the final coseismic slip model shown in Figure 6a. Each time window represents the slipped fault areas in the time interval indicated at the right of the windows, following the passage of the fastest rupture front. Slip larger than 30 cm is contoured at 30-cm intervals. See caption of Figure 3 for abbreviations used in the map.

GPS data, Çakır et al. [2003] concluded that the cosesimic rupture propagated offshore west of the Hersek peninsula for 30 km, with a slip amplitude that gradually decreased from 2 m to zero. Bos et al. [2004] inverted InSAR and GPS data, and showed that the rupture event extended beyond HYS with a slip of 0.7 m, while HYS slipped 1.4 m. Therefore, it appears that HYS also ruptured during the 1999 İzmit earthquake.

As five consecutive time windows are used in the modeling, we can comment on the change in slip rise time (or slip duration) and the rupture velocity across the fault plane by investigation of the individual slip contributions of each time window to the final coseismic slip model shown in Figure 6a. Figure 8 shows the slip distribution in each time window that resulted from the inversion. Each time window represents the slipped fault areas in the time interval indicated on the right side of the windows, following the passage of the fastest rupture front that propagated at velocities of 3.5 km/s for the central segment and 3.3 km/s for the other segments. A fault area that slips during the passage of the multiple time windows means longer slip duration for that fault area.

In general, each time window ends up having slip, but most of the slip occurred during the passage of the second and third time windows (Figure 8). This means that the data require significant delay relative to the maximum rupture velocities selected for the modeling: 3.5 km/s for the central segment, and 3.3 km/s for the other segments. The second time window, in which most of the slip took place, corresponds to the fault slippage during the passage of the rupture front traveling at velocities of approximately 2.9 km/s and 2.7 km/s for the central segment and the other segments, respectively. As most of the slip occurred during the passage of the second and third time windows, we can say that the main slip of the earthquake occurred with a rupture velocity varying in the range of 2.3 km/s to 2.9 km/s, while there is room for faster rupture velocities of up to 3.5 km/s. Smaller parts of the seismic moment release occurred with rupture velocities in the range of 1.8 km/s to 2.2 km/s.
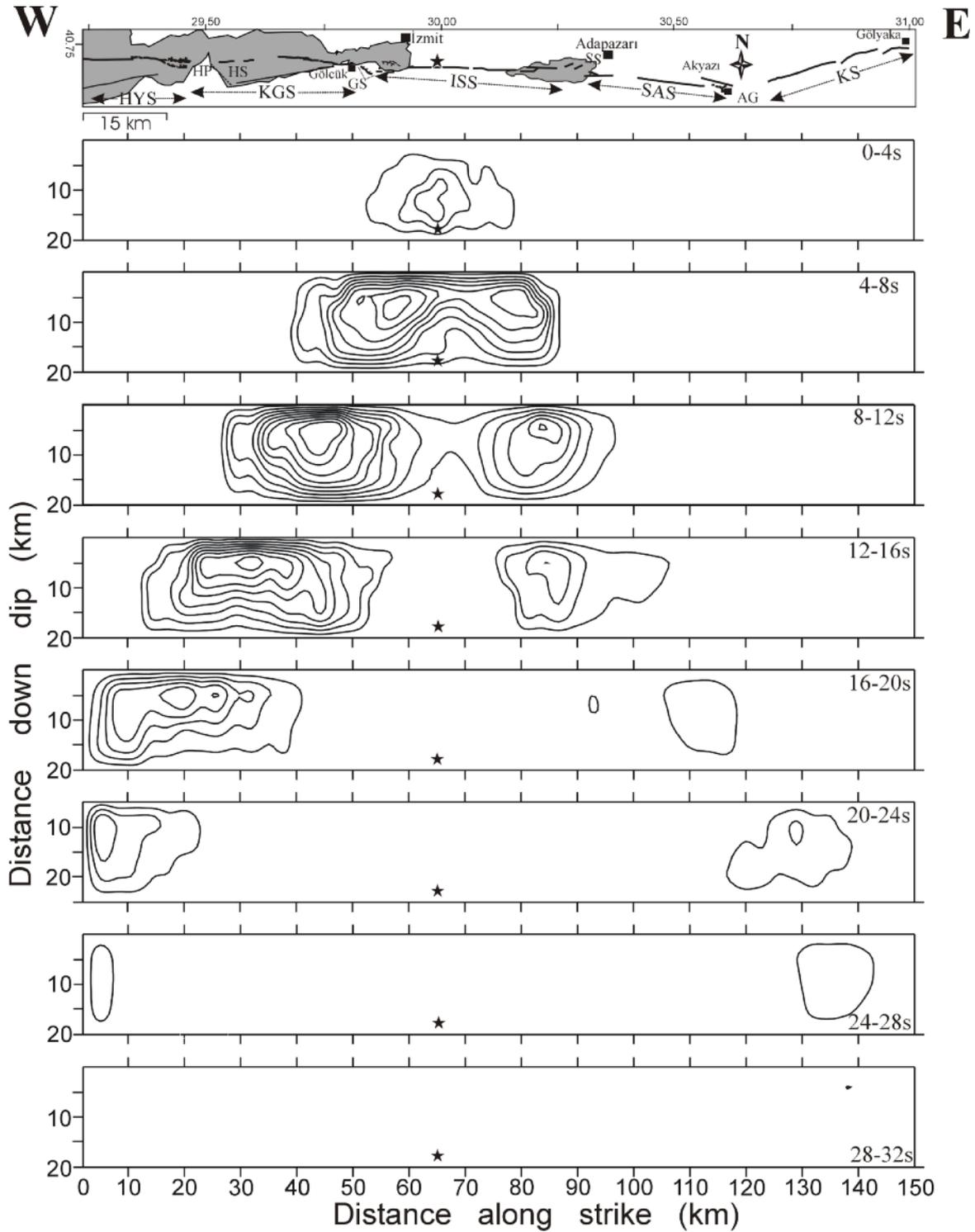
Figure 9. Space-time progression of the August 17, 1999, İzmit earthquake rupture given at intervals of 4 s, as labeled. Slip larger than 40 cm is contoured at 40-cm intervals. See caption of Figure 3 for abbreviations used in the map.

We now comment on the rise time over individual fault areas. Although all of the time windows end up with slip over the peak slip area of the eastern asperity, the significant slip occurred in the second and third time windows (Figure 8). Most of the slip over the peak slip area of the western asperity occurred in the first three time windows. This means that the data require shorter slip duration (about 4 s) for the eastern asperity than the western asperity, with an approximately 6 s slip duration. As significant slip over the hypocentral area

took place only in the second time window, this is another robust feature of the source process that results from the time window analysis. This means a much shorter slip rise time of ca. 2 s for the rupture initiation area, compared to the straddling large asperities. These findings largely agree with the spatial distribution of the slip duration that resulted from the near-field analysis, which have indicated a slip duration in the range of 3-5 s over the asperities, with the hypocentral area slipping in about 1 s [Bouchon et al. 2002].

For the 1999 İzmit earthquake, the rupture progression by means of slipping portions of the fault as a function of the absolute time in 4 s time slices can be constructed from the individual slip contributions of each time window shown in Figure 8. Several robust features can be noted from the time progression shown in Figure 9. There was relatively low seismic moment release in the hypocentral area within the first 4 s of the rupture, which was succeeded by failure of both of the large asperities in the time interval 4 s to 16 s. The seismic moment released due to the failure of both of the large asperities dominated the earthquake rupture, as seen from the moment rate function that resulted from the modeling (Figure 10). This can be interpreted as the existence of a smaller scale subevent, or subevents, that nucleated at the hypocentral area, just a few seconds before the major moment release. The smaller scale slip that preceded the main rupture indicates a rupture nucleation process, although its pattern might have been poorly resolved in the inversion due to its much smaller size compared to the main rupture and the resolution of the data used in the present study. As we further explore this issue below in our discussion, the nucleation process appears to go back to decades before the earthquake.

Following the failure of the large asperities, the rupture proceeded to the HYS segment in the west, in the time interval 12 s to 16 s (Figures 9, 10). After crossing Hersek stepover in the west, the rupture encountered Akyazı Gap in the east, in the time interval 16 s to 20 s. Then, the western-most section of the HYS segment failed, with a slip amplitude of >1 m, and the westward rupture virtually ended (in the time slice of 20 s to 24 s). This rupture stage over the HYS segment was also accompanied by rupture propagation to the KS segment in the east. The rupture across the KS segment lasted for about 12 s (in the time slices of 20 s to 32 s). The overall rupture process time was ca. 32 s, which is in agreement with the observed near-field recordings [Bouchon et al. 2002, Sekiguchi and Iwata 2002], as well as some teleseismic analyses [Vallee and Bouchon 2004]. The rupture evolution shown in Figure 9 also indicates that the geometrical fault discontinuities, such as Akyazı Gap and Sapanca, Gölcük and Hersek stepovers, perturbed the rupture propagation. Among these discontinuities, only Gölcük stepover, which is the boundary of the central and western segments of the model fault plane, is imposed as a discontinuity by the modeling parameterisation.

In general, deep slip in the slip-distribution model coincides with the observed surface displacement (Figures 3, 6). The large surface displacements in the vicinity of Gölcük town, the relatively low displacement observed over the hypocentral area and along KS, and the slip perturbation due to Akyazı Gap are well predicted from the modeling. The main difference is that the surface displacement of 5 m in the south of Adapazarı is under-predicted by the model. This
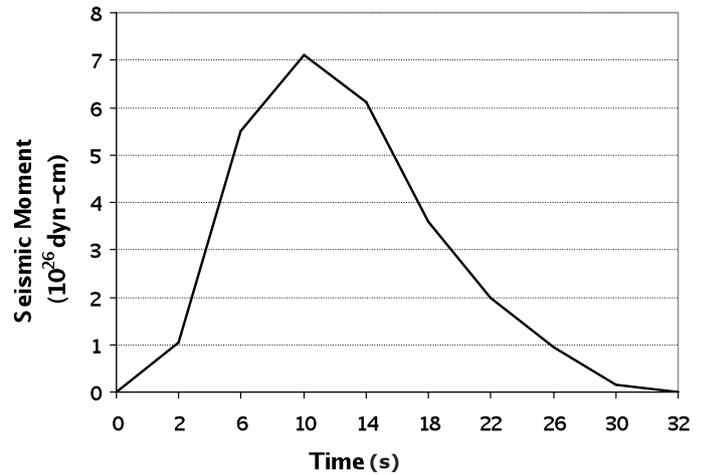

Figure 10. Far-field seismic moment–rate function inferred for the 1999 İzmit earthquake in the present study.

location corresponds to the eastern part of the eastern asperity with ca. 2.0 m slip. A plausible explanation for this slip difference is that the proposed dynamic triggering of the eastern asperity caused it to be mapped several kilometers west of its original location. Indeed, if failure of the eastern asperity takes place dynamically before the arrival of the fastest rupture front in our kinematic modeling, then the earlier seismic arrivals due to the dynamic failure would be approximated by the mapping of the eastern asperity much closer to the hypocenter than its original position. It can be considered that using faster rupture velocities in the kinematic modeling would overcome this problem. Of note, faster rupture velocities of up to 5 km/s have been used in the modeling. However, faster rupture velocities raised the misfit between the observed and predicted data (Table 3). Anyway, we show that the slip distribution resulted from model M10, with the supershear rupture velocity of 5.0 km/s for the central segment of the model fault in Figure 6b. The adoption of the supershear rupture velocity resulted in a larger slip amplitude of the western asperity, along with slightly eastward broadening of the rupture area of the eastern asperity. Nevertheless, the mapped surface slip in the south of Adapazarı is still under-predicted. At the same time, seismograms calculated from model M10 (Figure 6b) give poorer fits to the observed seismograms than model M1 (Table 3, Figure 6a). Therefore, we believe that model M1 as a better assumption of the 1999 İzmit rupture from the teleseismic velocity seismograms. We can claim that a dynamic triggering of the eastern asperity is vaguely preferred by the data.

Although there are some differences in the details, the slip model has many features in common with previously derived slip models (see Figure 11). In all of the models, the main slip area lies approximately between Hersek Peninsula in the west, and Adapazarı in the east. We first compared our slip model with the model of Delouis et al. [2002], who jointly inverted four datasets, near-field and far-field seismological data, and InSAR, GPS and geodetic data.
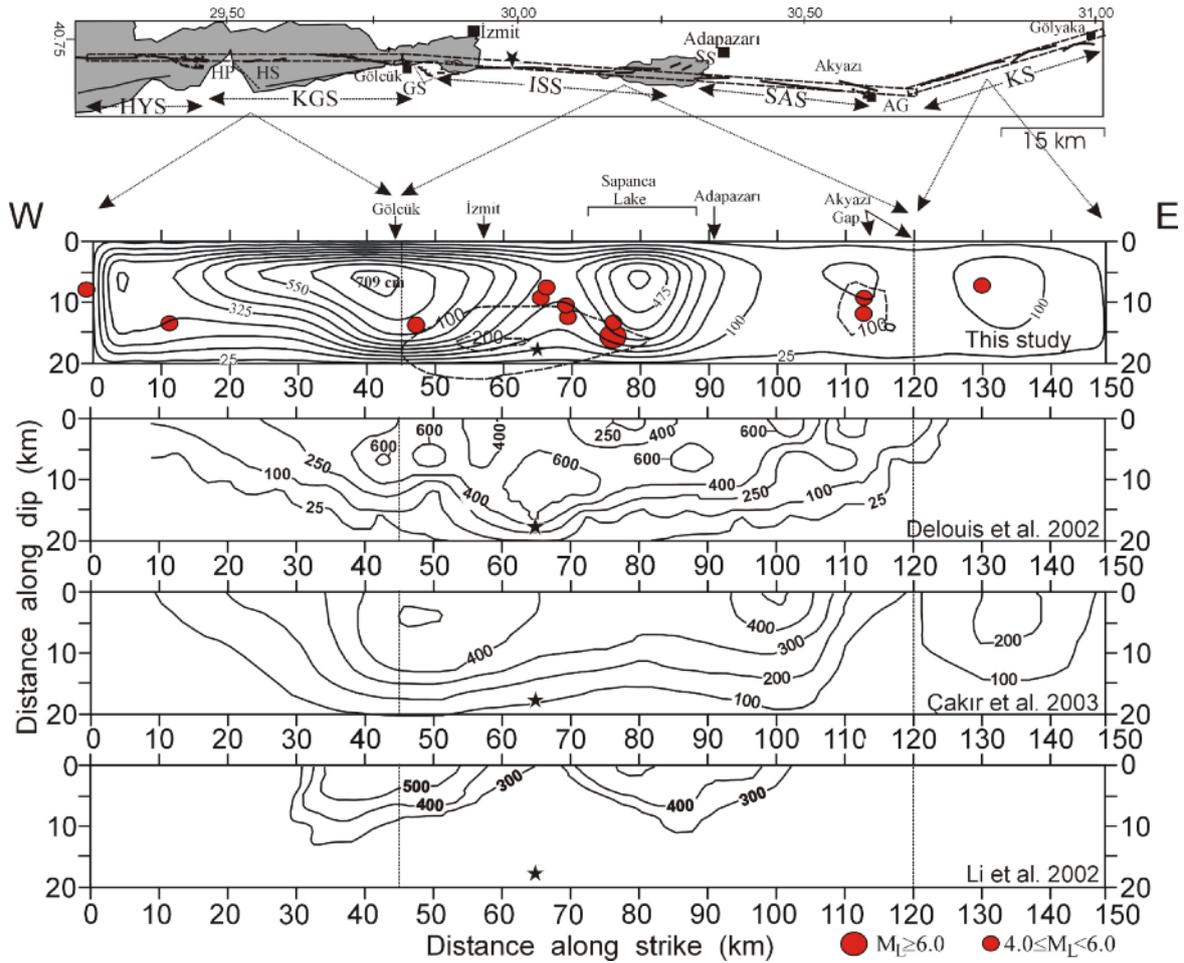
Figure 11. Comparison of the slip models arising in the present study for the 1999 İzmit earthquake with the slip models from previous studies. Thirty-day-long postseismic afterslip derived geodetically by Çakır et al. [2003] is indicated with broken-line contours in the slip model of the present study. The map of the surface rupture extent for correlating the slip distribution in the depth with the surface rupture trace is also shown. See caption of Figure 3 for abbreviations.

Delouis et al. [2002] inverted the joint dataset without and with a surface rupture constraint. Figure 11 shows features of their model without surface rupture constraint, because our modeling does not include the same constraint. However, in our slip model, the western asperity and EA coincide with high slip areas in their model, and the two models differs in amplitude of slip in the hypocentral area and over the HYS segment, and shallow slip located east of Sapanca Lake.

The differences in our slip distribution model compared with the model of Çakır et al. [2003] that was derived from the InSAR and GPS data is again a shallow, high-slip region east of Sapanca Lake and the slip amplitude over HYS (Figure 11). However, as the geodetic model features relatively low slip in the hypocentral area, this is in agreement with our study. The slip model of Li et al. [2002] that was derived from teleseismic displacements also indicates two large asperities and low slip in the hypocentral area, as in the present study (Figure 11). The locations and the extents of the large asperities in our model are in complete agreement with the 70-km-long main rupture zone that was derived by Vallee and Bouchon [2004] using teleseismic body and surface waves. The location of the eastern asperity of the slip

model exactly coincides with the main slip area of the slip model of Gülen et al. [2002], which resulted from rupture process analysis of the teleseismic *P* waves. Note that the models of Vallee and Bouchon [2004] and Gülen et al. [2002] are not shown in Figure 11.

Çakır et al. [2003] also mapped 30-day-long postseismic afterslip from the InSAR and GPS data along the rupture zone. The geodetic inversion revealed two areas of postseismic afterslip along the rupture zone, which are approximately projected on our slip model in Figure 11. The largest postseismic slip was mapped in the hypocentral area, with a peak slip amplitude slightly exceeding 2 m, while a relatively small postseismic slip area was derived beneath the Akyazı Gap, with a peak slip >1 m. The mapped large postseismic slip area supports the low slip area surrounding the rupture initiation, and it might reflect a slow deformation process for the closing of the slip deficit between the large asperities and hypocentral area following the coseismic rupture. As this area also experienced six ML ≥4.0 aftershocks, including the largest aftershock (the September 13, 1999, Sapanca earthquake, $M_L = 6.2$) [Özalaybey et al. 2002, Çakır et al. 2003] in the 2 month period, this further supports the low coseismic slip in
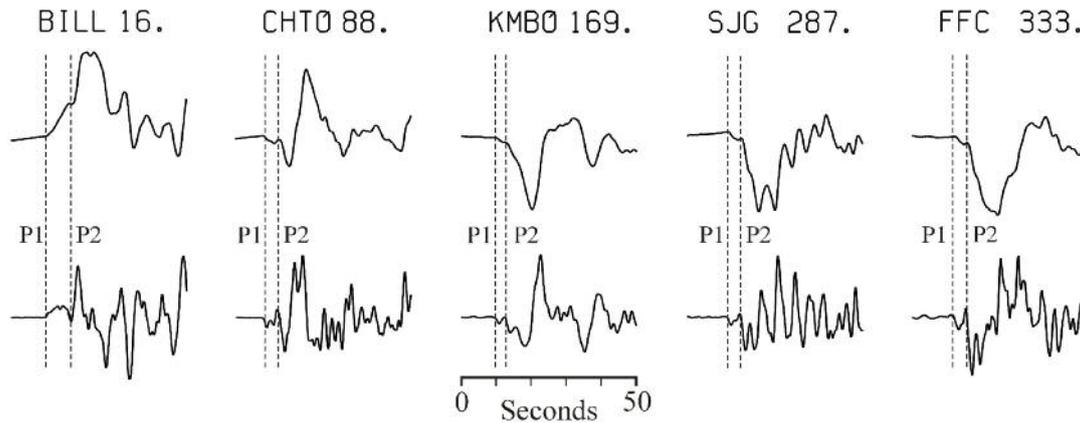
Figure 12. Far-field broadband displacement (top) and velocity (bottom) recordings for the 1999 İzmit earthquake from several stations. The records are bandpass filtered with corner frequencies at 0.01 Hz to 1.0 Hz. A precursory source feature that appears as a small shoulder before the main *P* displacement pulse and as a tiny pulse before the major *P* velocity pulses is clearly visible. The numbers on the right of the station names indicate azimuths, clockwise from the North. Vertical broken line labelled as P1 and P2, the first and the major *P*-wave energy arrivals at each station, respectively.

the area, and provides evidence that a part of the postseismic slip occurred seismically (Figure 11).

The recordings of the many earthquakes, and particularly of the large ones, have been reported to have emergent rather than abrupt onsets, which indicates precursory rupture growth or continuous increases in the slip velocity that led to the main ruptures [Brune 1979, Abercrombie and Mori 1994, Ellsworth and Beroza 1995, Dodge and Beroza 1996, Shibazaki et al. 2002]. The time interval between the onset of the relatively weak ground motion of these precursory source features and the initiation of the sudden arrival of the strong ground motion of the following ensuing main rupture in velocity seismograms is referred to as the seismic nucleation process. The weak ground motion has been generally related to an immediate subevent, or subevents.

As seen from the moment-rate function that resulted from the modeling, the seismic moment release due to failure of the large asperities dominates the earthquake rupture, following a gradually rising, but relatively small, seismic moment release (Figure 10). This can be interpreted as a smaller scale subevent, or subevents, that nucleated at the hypocentral area, just a few seconds before the major moment release. The precursory source features can be directly observed from the far-field *P*-wave displacement and velocity records at several stations shown in Figure 12. Note that a small shoulder before the major *P*-wave displacement pulse and a tiny velocity pulse before the large velocity pulses clearly indicate a precursory source feature prior to the arrival of the major *P*-wave energy. Delayed large amplitude arrivals with respect to rupture initiation are resolved as an abrupt increase in the seismic moment–rate function shown in Figure 10 following a slow moment release in the initial section. This emergent onset of the seismic wave arrivals is also discernable from the near-field seismograms (see: Figure 3 of Sekiguchi and Iwata [2002], Figure 10 of Polat et al. [2002], Bouchon et al. [2011]). As Figure 9 can be considered as an image of the variation in the slip velocity with time, it

should have a sign or presence of the nucleation process, or a gradual rise in the slip velocity before a sudden increase. The data resolution does not allow the details of the gradual rise of slip velocity or the nucleation phase to be mapped in Figure 9, but rather it indicates the presence of a slow slip velocity phase within the first 4 s, and its abrupt growth after this phase. These observations suggest a seismic nucleation phase for the 1999 İzmit earthquake. Detailed analysis by Bouchon et al. [2011] identified at least two smaller events that immediately preceded the earthquake, as far as the resolution of the near-source recordings allows.

There are some clues that the nucleation phase of the 1999 İzmit earthquake has root in the preseismic period. The hypocentral area has been notable for its background seismicity cluster decades before the 1999 İzmit earthquake [Crampin et al. 1985, Evans et al. 1985, Evans et al. 1987, Gülen et al. 2002, Barış et al. 2002]. As seen from the seismicity data recovered from the catalog of the Kandilli Observatory and Earthquake Research Institute, a notable seismicity cluster is seen in the epicentral area during the preceding year (Figure 13). From the seismicity along the rupture zone that covers the time period between 1991 and 1999.5, Öncel and Wilson [2007] reported anomalous changes in the seismicity parameters at 2-3-year time intervals. In the time period 1.5 years to 3 years prior to the earthquake, they found that the seismicity became increasingly clustered, accompanied by a rise in the *b* value from 1.6 to 2.26, as compared to the previous phase, which indicates increased levels of low magnitude seismicity. They related these observations with an increased probability of a forthcoming large earthquake.

Özalaybey et al. [2002] noted eight M ≤2.5 foreshocks in the hours that preceded the mainshock hypocentral time, and in close vicinity to the mainshock rupture initiation point. Özalaybey et al. [2002] also reported that the seismograms of these foreshocks at a nearby station (about 13 km away from the hypocenter) differed in their frequency contents, and longer period ground motions were dominating as time
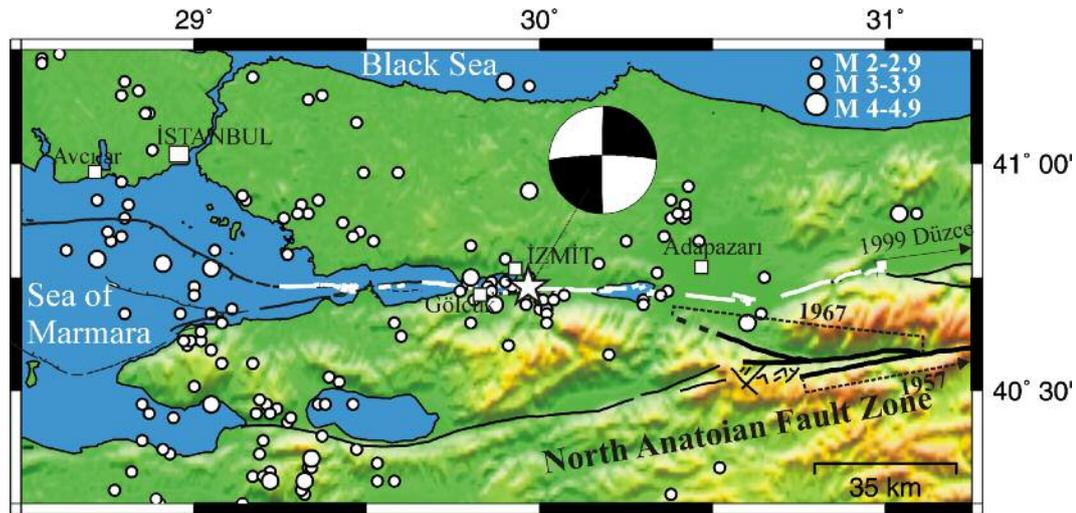
Figure 13. Seismicity of the August 17, 1999, İzmit earthquake source region during the year before the earthquake. The seismicity data were recovered from the catalog of Kandilli Observatory and the Earthquake Research Institute. The mapped surface ruptures (thick white lines) and the focal mechanism of the earthquake are also shown. White star, epicentre. The onshore fault extents are drawn from Şaroğlu et al. [1992], while the offshore extents are drawn from Armijo et al. [2002].

passed. This observation is related to the increasing dilatancy in the nucleation area, which caused more wave attenuation. Bouchon et al. [2011] showed that the there had been a phase of slow slip process that started 44 min before the earthquake at the hypocentral location, which were accompanied by a succession of repeating events that emitted identical signals. The slow slip process was followed by accelerating the slip 2 min before the earthquake. Note that this area also correlates with the maximum postseismic slip region [Çakır et al. 2003] and hosts the largest aftershock, along with several other $M_L \geq 4.0$ aftershocks (Figure 11).

All of the observations given above suggest a complex nucleation process for the 1999 İzmit earthquake that goes back to decades before the main rupture and that climaxed in the hours prior to the main rupture, with the occurrence of the foreshocks, the last of which turned into the mainshock rupture. This implies that a preslip nucleation model is consistent with the seismic nucleation phase of the 1999 İzmit earthquake. In the preslip nucleation model, the main rupture was caused by a preceding episodic aseismic slip process over a limited fault area or fault patch that widened progressively [Ellsworth and Beroza 1995]. The aseismic slip gradually accelerated, until the preslip patch reached a critical size. The aseismic slip was accompanied by small earthquakes. The reported rise in the *b* value in the period 1.5 years to 3 years prior to the earthquake might have been an indication of the episodic aseismic slip process, since aseismic slip is associated with high *b* values [Amelung and King 1997, Öncel and Wilson 2007].

5. Conclusions

Teleseismic *P* and *SH* velocity waveforms of the August 17, 1999, İzmit earthquake were inverted to obtain a finite-fault coseismic slip model of the earthquake. The modeling

has yielded a very heterogeneous coseismic slip model for the earthquake, with a total seismic moment of 2.6×10^{20} Nm. The coseismic slip model suggests that: 1) the main rupture area was ca. 70 km in length and comprised the rupture of two large asperities (eastern and western asperities) located both sides of the hypocenter, with peak slip reaching 7 m in the depth range 4 km to 9 km; 2) the slip was relatively low (1-2 m) in the hypocentral region; 3) there was a prominent slip gap between the eastern asperity and the Karadere fault segment that coincided with the observed surface rupture gap known as Akyazı Gap; 4) the slip across the Karadere fault segment was about 1.5 m; 5) the rupture extended offshore west of Hersek Peninsula to the eastern tip of the Çınarcık Basin, with relatively low mean slip (ca. 2 m); and 6) the rupture was completely dextral, with a total rupture time of 32 s.

The overall coseismic slip pattern appears to be greatly effected by the fault zone segmentation and discontinuities. Prominent fault zone discontinuities, namely Sapanca, Gölcük and Hersek stepovers and Akyazı Gap, substantially affected the coseismic slip pattern and slip amplitudes not only on the surface, but also deep in the crust. The main seismic moment release occurred during the failure of the large asperities between 4 s and 16 s. Finally, discussion of some published observations and the results yielded by this study indicate that the earthquake had a seismic nucleation phase.

References

Abercrombie, R., and J. Mori (1994). Local observations of the onset of a large earthquake: 28 June 1992 Landers, California, B. Seismol. Soc. Am., 84, 725-734.

Ambraseys, N.N., and C.F. Finkel (1991). Long-term seis-

micity of stanbul and of the Marmara Sea region, Terra Nova, 3, 527-539.

Ambraseys, N. (2002). The seismic activity of the Marmara Sea region over the last 2000 years, B. Seismol. Soc. Am., 92, 1-18.

Amelung, F., and G. King (1997). Earthquake scaling laws for creeping and non-creeping faults, Geophys. Res. Lett., 24, 507-510.

Anderson, J.G., H. Sucuoğlu, A. Erberik, T. Yılmaz, E. Inan, E. Durukal, M. Erdik, R. Anooshehepoor, J.N. Brune and S.-D. Ni (2000). Implications for seismic hazard analysis, In: T.L. Youd, J.P. Bardet and J.D. Bray (eds.), Kocaeli, Turkey, earthquake of August 17, 1999, Earthq. Spectra, 16, 113-137; doi:http://dx.doi.org/10.1193/1.1586150.

Armijo, R., B. Meyer, S. Navarro, G. King and A. Barka (2002). Asymmetric slip partitioning in the Sea of Marmara pull-apart: a clue to propagation processes of the North Anatolian Fault?, Terra Nova, 14, 80-86.

Armijo, R., N. Pondard, B. Meyer, G. Uçarku , B.M. de Lépinay, J. Malavieille, S. Dominguez, M.A. Gustcher, S. Schmidt, C. Beck, N. Çağatay, Z. Çakır, C. Imren, K. Eris, B. Natalin, S. Özalaybey, L. Tolun, I. Lefèvre, L. Seeber, L. Gasperini, C. Rangin, O. Emre and K. Sarikavak (2005). Submarine fault scarps in the Sea of Marmara pull-apart (North Anatolian Fault): implications for seismic hazard in stanbul, Geochem. Geophy. Geosy., 6, Q06009; doi:10.1029/2004GC000896.

Aydın, A., and D. Kalafat (2002). Surface ruptures of the 17 August and 12 November 1999 zmit and Düzce earthquakes in Northwestern Anatolia, Turkey: their tectonic and kinematic significance and the associated damage, B. Seismol. Soc. Am., 92, 95-106.

Barış, Ş., A. Ito, S.B. Üçer, Y. Honkura, N. Kafadar, R. Pekta , T. Komut and A.M. Işıkara (2002). Microearthquake activity before the zmit Earthquake in the eastern Marmara Region, Turkey (1 January 1993-17 August 1999), B. Seismol. Soc. Am., 92, 394-406.

Barka, A., and K. Kandisky-Cade (1988). Strike-slip fault geometry in Turkey and its influence on earthquake activity, Tectonics, 7, 663-684.

Barka, A. (1996). Slip distribution along the North Anatolian Fault associated with the large earthquakes of the period 1939 to 1967, B. Seismol. Soc. Am., 86, 1238-1254.

Barka, A., E. Altunel, G. Sunal, Z. Çakır, A. Dikba , B. Yerli, R. Armijo, B. Meyer, J.B. de Chabalier, J.R. Rockwell, J.R. Dolan, R. Hartleb, T. Dawson, S. Christofferson, A. Tucker, T. Fumal, R. Langridge, H. Stenner, W. Lettis, J. Bachhubber and W. Page (2002). The surface rupture and slip distribution of the 17 August 1999 İzmit earthquake (M 7.4), North Anatolian Fault, B. Seismol. Soc. Am., 92, 43-60.

Bos, A.G., S. Usai and W. Spakman (2004). A joint analysis of GPS motions and InSAR to infer the coseismic surface deformation of the zmit, Turkey earthquake, Geophys. J. Int., 158, 849-863.

Bouchon, M., M.N. Toksöz, H. Karabulut, M.P. Bouin, M. Dietrich, M. Aktar and M. Edie (2002). Space and time evolution of rupture and faulting during the 1999 İzmit (Turkey) earthquake, B. Seismol. Soc. Am., 92, 256-266.

Bouchon, M., H. Karabulut, M. Aktar, S. Özalaybey, J. Schmittbuhl and M.P. Bouin (2011). Extended nucleation of the M_W = 7.6 zmit earthquake, Science, 331, 877-880.

Brune, J. (1979). Implications of earthquake triggering and rupture propagation for earthquake prediction based on premonitory phenomena, J. Geophys. Res., 84, 2195-2198.

Çakır, Z., J.B. Chabalier, R. Armijo, B. Meyer, A. Barka and G. Peltzer (2003). Coseismic and early post-seismic slip associated with the 1999 zmit earthquake (Turkey), from SAR interferometry and tectonic field observations, Geophys. J. Int., 155, 93-110.

Cormier, M.H., L. Seeber, C.M.G. McHugh, A. Polonia, N. Çağatay, Ö. Emre, L. Gasperini, N. Görür, G. Bortoluzzi, E. Bonatti, W.B.F. Ryan and K.R. Newman (2006). North Anatolian Fault in the Gulf of İzmit (Turkey): rapid vertical motion in response to minor bends of a nonvertical continental transform, J. Geophys. Res., 111, B04102; doi:10.1029/2005JB003633

Crampin, S., R. Evans and S.B. Üçer (1985). Analysis of records of local earthquakes: the Turkish Dilatancy Projects (TDP1 and TDP2), Geophys. J. Roy. Astr. S., 83, 1-16.

Delouis, B., D. Giardini, P. Lundgren and J. Salichon (2002). Joint inversion of InSAR, GPS, teleseismic, and strong-motion data for the spatial and temporal distribution of earthquake slip: application to the 1999 zmit mainshock, B. Seismol. Soc. Am., 92, 278-299.

Dodge, A.D., and G. C. Beroza (1996). Detailed observations of California foreshock sequences: implications for the earthquake initiation process, J. Geophys. Res., 101, 22371-22392.

Ellsworth, W.L., and G.C. Beroza (1995). Seismic evidence for a seismic nucleation phase, Science, 268, 851-855.

Ellsworth, W.L., and M. Celebi (1999). Near field displacement time histories of the M 7.4 Kocaeli (zmit), Turkey, earthquake of August 17, 1999, EOS Trans. AGU, F648.

Evans, R., I. Asudeh, S. Crampin and S.B. Üçer (1985). Tectonics of the Marmara Sea region of Turkey: new evidence from micro-earthquake fault plane solutions, Geophys. J. Roy. Astr. S., 83, 47-60.

Evans, R., D. Beamish, S. Crampin and S.B. Üçer (1987). Turkish Dilatancy Project (TDP3): multidisciplinary studies of a potential earthquake source region, Geophys. J. Roy. Astr. S., 91, 265-286.

Flerit, F., R. Armijo, G.C.P. King, B. Meyer and A. Barka (2003). Slip partitioning in the Sea of Marmara pull-apart determined from GPS velocity vectors, Geophys. J. Int., 154, 1-7.

Gasperini, L., A. Polonia, G. Bortoluzzi, P. Henry, X. Le Pichon, M. Tryon, N. Çağatay and L. Geli (2011). How far did the surface rupture of the 1999 İzmit earthquake reach in Sea of Marmara?, Tectonics, 30, TC1010; doi:10.1029/2010TC002726.

Gülen, L., A. Pınar, D. Kalafat, N. Özel, G. Horasan, M. Yılmazer and A. M. Işıkara (2002). Surface fault breaks, aftershock distribution, and rupture process of the 17 August 1999 İzmit, Turkey, earthquake, B. Seismol. Soc. Am., 92, 230-245.

Hartzell, S.H., and T.H. Heaton (1983). Inversion of strong-ground motion and teleseismic wave form data for the fault rupture history of the 1979 Imperial Valley, California, earthquake, B. Seismol. Soc. Am., 73, 1553-1583.

Hartzell, S.H., and M. Iida (1990). Source complexity of the 1987 Whitter Narrows, California, earthquake from the inversion of strong-motion waveforms, J. Geophys. Res., 95, 12475-12485.

Hartzell, S.H., G.S. Stewart and C. Mendoza (1991). Comparison of L1 and L2 norms in a teleseismic waveform inversion for the slip history of the Loma Prieta, California, earthquake, B. Seismol. Soc. Am., 81, 1518-1539.

Horasan, G., L. Gülen, A. Pınar, D. Kalafat, N. Özel, H.S. Kuleli and A.M. Iıkara (2002). Lithospheric structure of the Marmara and Aegean regions, Western Turkey, B. Seismol. Soc. Am., 92, 322-329.

Hubert-Ferrari, A., A. Barka, E. Jacques, S.S. Nalbant, B. Meyer, R. Armijo, P. Tapponier and G.C.P. King (2000). Seismic hazard following the 17 August 1999 İzmit earthquake, Nature, 404, 269-273.

Langer, C.J., and S. Hartzell (1996). Rupture distribution of the 1977 western Argentina earthquake, Phys. Earth Planet. In., 94, 121-132.

Langston, C.A., and D.V. Helmberger (1975). A procedure for modelling dislocation sources, Geophys. J. Roy. Astr. S., 42, 117-130.

Lawson, C.L., and R.J. Hanson (1974). Solving least square problem, Englewood Cliffs: Prentice-Hall, New Jersey.

Lettis, W., J. Bachhuber, R. Witter, C. Brankman, C.E. Randolph, A. Barka, W.D. Page and A. Kaya (2002). Influence of releasing stepovers on surface fault rupture and fault segmentation: examples from the 17 August 1999 İzmit earthquake on the North Anatolian Fault, Turkey, B. Seismol. Soc. Am., 92, 19-42.

Li, X., V.F. Cormier and M.N. Toksöz (2002). Complex source process of the 17 August 1999 zmit, Turkey, earthquake, B. Seismol. Soc. Am., 92, 267-277.

Lorenzo-Martin, F., F. Roth and R. Wang (2006). Elastic and inelastic triggering of earthquakes in the North Anatolian Fault zone, Tectonophysics, 424, 271-289.

McClusky, S., S. Balassanian, A. Barka, C. Demir, S. Ergintav, I. Georgiev, O. Gürkan, M. Hamburger, K. Hurst, H. Kahle, K. Kastens, M. Nadariya, A. Ouzounis, D. Par-

adissis, Y. Peter, M. Prilepin, R. Reilinger, I. Sanli, H. Seeger, A. Tealeb, M.N. Toksöz and G. Veis (2000). GPS constraints on plate kinematics and dynamics in the Eastern Mediterranean and Caucasus, J. Geophys. Res., 105, 5695-5719.

Meade, B.J., B.H. Hager, S.C. McClusky, R.E. Reilinger, S. Ergintav, O. Lenk, A. Barka and H. Özener (2002). Estimates of seismic potential in the Marmara Sea region from block models of secular deformation constrained by global positioning system measurements, B. Seismol. Soc. Am., 92, 208-215.

Mendoza, C. (1993). Coseismic slip of two large Mexican earthquakes from teleseismic body waveforms: implications for asperity interaction in the Michoacan plate boundary segment, J. Geophys. Res., 93, 8197-8210.

Mendoza, C. (1995). Finite-fault analysis of the 1979 March 14 Petetlan, Mexico, earthquake using teleseismic P wave forms, Geophys. J. Int., 121, 675-683.

Nyst, M., and W. Thatcher (2004). New constraints on the active tectonic deformation of the Aegean, J. Geophys. Res., 109, B11406; doi:10.1029/2003JB002830.

Öncel, A.O., and T. Wilson (2007). Anomalous seismicity preceding the 1999 İzmit event, NW Turkey, Geophys. J. Int., 169, 259-270.

Özalaybey, S., M. Ergin, M. Aktar, C. Tapırdamaz, F. Biçmen and A. Yörük (2002). The 1999 zmit earthquake sequence in Turkey: seismological and tectonic aspects, B. Seismol. Soc. Am., 92, 376-386.

Parsons, T., S. Toda, R.S. Stein, A. Barka and J.H. Dieterich (2000). Heightened odds of large earthquakes near stanbul: an interaction-based probability calculation, Science, 288, 661-665.

Parsons, T. (2004). Recalculated probability of M ≥7 earthquakes beneath the Sea of Marmara, Turkey, J. Geophy. Res., 109, B05304; doi:10.1029/2003JB002667.

Polat, O., H. Haessler, A. Cisternas, H. Philip, H. Eyidoğan, M. Aktar, M. Frogneux, D. Comte and C. Gürbüz (2002). The İzmit (Kocaeli), Turkey, earthquake of 17 August 1999: previous seismicity, aftershocks and seismotectonics, B. Seismol. Soc. Am., 92, 361-375.

Pondard, N., R. Armijo, G.C.P. King, B. Meyer and F. Flerit (2007). Fault interactions in the Sea of Marmara pull-apart (North Anatolian Fault): earthquake clustering and propagating earthquake sequences, Geophys. J. Int., 171, 1185-1197; doi: 10.1111/j.1365-246X.2007.03580.x.

Reilinger, R., S. Ergintav, R. Bürgman, S. McClusky, O. Lenk, A. Barka, O. Gürkan, L. Hearn, K.L. Feigl, R. Çakmak, B. Aktu, H. Özener and M.N. Toksöz (2000). Coseismic and postseismic fault slip for the 17 August 1999, M = 7.5, zmit, Turkey earthquake, Science, 289, 1519-1524.

Reilinger, R., S. McClusky, P. Vernant, S. Lawrence, S. Ergintav, R. Cakmak, H. Ozaener, F. Kadirov, I. Guliev, R. Stepanyan, M. Naradiya, G. Hahubia, S. Mahmoud, K. Sakr,

A. ArRajehi, D. Paradissis, A. Al-Aydrus, M. Prilepin, T. Guseva, E. Evren, A. Dmitrotsa, S. V. Filikov, F. Gomez, R. Al-Ghazzi and G. Karam (2006). GPS constraints on continental deformation in the Africa–Arabia–Eurasia continental collision zone and implications for the dynamics of plate interactions, J. Geophys. Res., BO5411; doi:10.1029/20 05JB0 0 4051.

Şaroğlu, F., Ö. Emre and İ. Kuşçu (1992). Active fault map of Turkey, General Directorate of Mineral Research and Exploration, Ankara, Turkey.

Sekiguchi, H., and T. Iwata (2002). Rupture process of the 1999 Kocaeli, Turkey, earthquake estimated from strong-motion waveforms, B. Seismol. Soc. Am., 92, 300-311.

Şengör, A.M.C., O. Tüysüz, C. Imren, M. Sakınç, H. Eyidoğan, N. Görür, X. Le Pichon and C. Rangin (2005). The North Anatolian Fault: a new look, Annu. Rev. Earth Pl. Sc., 33, 37-112; doi: 10.1146/annurev.earth.32.101802. 120415.

Shibazaki, B., Y. Yoshida, M. Nakamura and H. Katao (2002). Rupture nucleations in the 1995 Hyogo- Nanbu earthquake and its large aftershocks, Geophys. J. Int., 149, 572-588.

Stein, R., A. Barka and J.H. Dietrich (1997). Progressive failure on the North Anatolian Fault since 1939 by earthquake stress triggering, Geophys. J. Int., 128, 594-604.

Tibi, R., G. Bock, Y. Xia, M. Baumbach, H. Grosser, C. Milkerit, S. Karakisa, S. Zünbül, R. Kind and J. Zschau (2001). Rupture process of the August 17 zmit and November 12, 1999 Düzce (Turkey) earthquakes, Geophys. J. Int., 144, F1-F7.

Toksöz, M.N., A.F. Shakal and A.J. Micheal (1979). Space-time migration of earthquakes along the North Anatolian Fault Zone and seismic gap, Pure Appl. Geophys., 117, 1258-1270.

Uçarku , G., Z. Çakır and R. Armijo (2011). Western termination of the Mw 7.4, 1999 zmit earthquake rupture: implication for the expected large earthquake in the Sea of Marmara, Turkish J. Earth Sci., 20, 379-394.

Utkucu, M., S. Nalbant, J. McClusky, S. Steacy and Ö. Alptekin (2003). Slip distribution and stress changes associated with the 1999 November 12, Düzce (Turkey) earthquake (Mw = 7.1), Geophys. J. Int., 153, 229-241.

Vallee, M., and M. Bouchon (2004). Imaging coseismic rupture in far by slip patches, Geophys. J. Int., 156, 615-630.

Wald, D.J., and T.H. Heaton (1994). Spatial and temporal distribution of slip for the 1992 Landers, California, earthquake, B. Seismol. Soc. Am., 84, 668-691.

*Corresponding author: Hatice Durmuş,
Sakarya University, Esentepe Campus, Department of Geophysics,
Sakarya, Turkey; email: herguven@sakarya.edu.tr.